JPE 19-1-24

https://doi.org/10.6113/JPE.2019.19.1.254
ISSN(Print): 1598-2092 / ISSN(Online): 2093-4718

Seamless Mode Transfer of Utility Interactive Inverters Based on Indirect Current Control

Kyungbae Lim*, Injong Song*, Jaeho Choi†, Hyeong-Jun Yoo**, and Hak-Man Kim**

†,*School of Electrical Engineering, Chungbuk National University, Cheongju, Korea
**Department of Electrical Engineering, Incheon National University, Incheon, Korea

Abstract

This paper proposes an indirect current control technique based on a proportional resonant (PR) approach for the seamless mode transfer of utility interactive inverters. Direct-current and voltage hybrid control methods have been used for inverter control under grid-connected and islanded modes. A large bandwidth can be selected due to the structure of single-loop control. However, this results in poor dynamic transients due to sudden changes of the controller during mode changes. Therefore, inverter control based on indirect current is proposed to improve the dynamic transients by consistently controlling the output voltage under all of the operation modes. A PR-based indirect current control topology is used in this study to maintain the load voltage quality under all of the modes. The design processes of the PR-based triple loop are analyzed in detail while considering the system stability and dynamic transients. The mode transfer techniques are described in detail for both sudden unintentional islanding and islanded mode voltage quality improvements. In addition, they are described using the proposed indirect control structure. The proposed method is verified by the PSiM simulations and laboratory-scale VDER-HILS experiments.

Key words: Indirect current control, PR control, Seamless transfer, Unintentional islanding, Utility interactive inverter

I. INTRODUCTION

Microgrids integrate renewable energy sources (RESs) such as photovoltaic generators, wind power generators, fuel cells and other power sources with engine generators and batteries. Microgrids have been widely applied because of their flexibility and capability to supply power reliably [1]-[6]. Among them, inverter based distributed generation (DG) has been one of the main types of equipment in microgrids due to its accurate power conversion. Therefore, utility interactive inverter control has recently become one of the most popular issues in the research of microgrids.

An inverter in the grid-connected mode must supply power to a grid or local loads with the acceptable level of power quality [7]. Therefore, a DG-based inverter can be defined as a current source or a sub-power source [8]. However, an inverter needs to be operated as a voltage source when strategic intentional islanding operation is needed or the recloser switch is opened at the point of common coupling (PCC) due to a sudden grid fault or grid quality degradation. This is necessary because the inverter has to supply the full local load demand in place of the main grid under the islanded mode [9]. On the other hand, the inverter needs to change the mode from the islanded mode to the grid-connected mode when the grid has recovered from a pre-fault state or when the intentional islanding is no longer necessary. During these transitions, the inverter has to keep the power quality within an allowable range to avoid load damage or decreases in the load span due to an unrated local load voltage during mode transitions.

There have been a number of studies on mode transition techniques to maintain power quality during mode transfers. Current control and voltage control have been used in both the grid-connected mode and the islanded mode [10]-[12]. However, the load voltage quality was fairly degraded during the transient state of the mode transfer process, and the regulation performance of the load voltage was quite sensitive to changes of the operation process, especially when islanding occurs. A droop-based voltage control scheme has also been proposed [13]. The droop-based inverter was defined as a

Manuscript received Sep. 13, 2018; accepted Oct. 18, 2018
Recommended for publication by Associate Editor Kyo-Beum Lee.
†Corresponding Author: choi@cbnu.ac.kr
Tel: +82-43-261-2425, Fax:+82-43-276-7217,Chungbuk Nat'l Univ.
*School of Electrical Eng., Chungbuk National University, Korea
**Dept. of Electrical Eng., Incheon National University, Korea

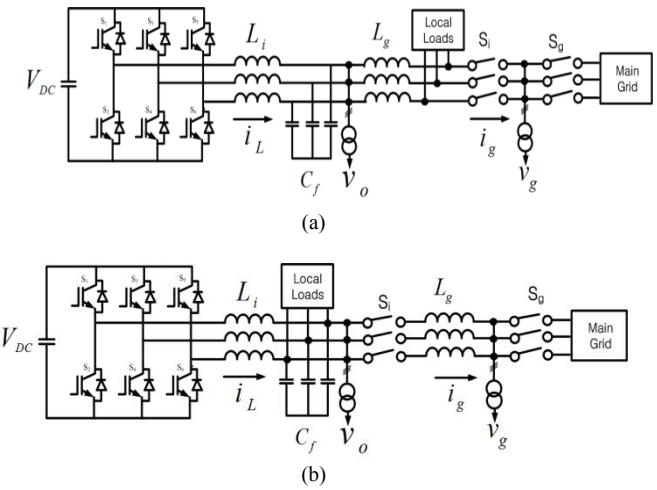

Fig. 1. System configuration according to location of the local load: (a) After grid side inductor; (b) Before grid side inductor.

voltage source under both the islanded and gird-connected modes. It was possible to guarantee the load voltage quality with this method during operation mode transitions. However, the dynamic performance was not very good.

The concept of indirect current control was introduced to improve the power quality during mode transitions when compared to the conventional control techniques presented in [14]-[17]. In comparison to the direct current control used in the grid-connected mode, the output value of the current loop in indirect current control becomes the reference value of the inner voltage loop. This means that the inverter output voltage can be controlled consistently regardless of the operation modes, unlike direct current control. Therefore, the direct current control can have a wider control bandwidth due to the single control-loop structure. However, it can cause poor mode dynamic transients when compared to the case where the direct current control is used. Therefore, the indirect current control requires additional techniques to achieve better mode transition dynamics due to the multiple quality-degradation factors, such as sudden unintentional islanding and a complicated system structure.

The indirect current control method was designed as a calculation method for capacitor reference voltage based on a sine and cosine table [14], [15]. The correct reference voltage assignment was obtained by considering the voltage drop of both the grid-side inductor and the line impedance. The local load voltage quality was greatly improved when compared to the case when only a single voltage and current controller was used in the islanded and grid-connected modes. However, this method had some drawbacks in that the capacitor reference generation method was slightly complicated, which can become a more serious issue when the role of the control is extended to non-linear load compensation. This can occur because the expected capacitor reference voltage has to be calculated while considering the harmonic voltage drop of the grid-side inductor.

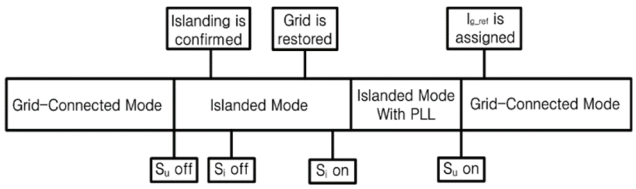

Fig. 2. Mode transition sequence loop described in [16], [17].

To avoid mismatch between the inverter output voltage and the load voltage, an indirect current control method was proposed, which locates local loads at the output of an LC filter [16], [17]. Fig. 1(a) and 1(b) represent the system configuration depending on the location of the local load after the grid side inductor [14], [15] and before the grid side inductor [16], [17], respectively. If the local load is located after the grid side inductor, as shown in Fig. 1(a), the current control is difficult due to the voltage drop of the grid-side inductor. On the other hand, if the local load is located before the grid side inductor, the direct load voltage regulation is possible using the system configuration shown in Fig. 1(b). However, it can cause a slight voltage magnitude tracking degradation due to the presence of a grid-side inductor between the local load and the grid. However, this tracking degradation does not affect much in a high capacity system where the current is generally high. This is because the filter inductor of the inverter is generally designed to have a smaller inductance value when the system capacity becomes larger.

In [16], [17], an indirect current control method based on the synchronous d-q frame control was proposed. In this method, the controller design included limiters for each of the d-q values, which were outputs of the grid current loop. This method can counter the control failures resulting from controller changes such as changes of the operation mode since the indirect current control always regulates the output voltage as the inner loop of the outer current loop. However, the quality of the steady-state output voltage deteriorated slightly because the inverter output voltage in islanded mode had to be operated with threshold values for the limiter. Fig. 2 shows the mode transition sequence based on the system configuration in Fig. 1(b).

In [18], [19], indirect current control based on the proportional resonant (PR) control [20]-[28] was proposed. The location of the load is same as that in [17]. The PR control in the stationary reference frame was chosen as the control technique because it can compensate for positive and negative sequence components with only one controller, unlike the PI controller. Additionally, it has more advantages for the compensation of the harmful effects caused by non-linear loads because the control design for compensating harmonics was a lot simpler than compensation based on the PI controller. The load voltage quality can be guaranteed using the proposed method during a mode transfer. However, the method included only intentional islanding transfer for

strategic islanding operation without considering unintentional islanding events due to the sudden opening of a recloser switch. Therefore, there is a strong demand for a PR-based seamless transfer technique that includes unintentional islanding operation because of sudden opening of a recloser switch due to grid faults, which would increase the reliability in all of the operation modes of a utility interactive inverter.

In this study, the PR-based triple-loop indirect current controller in [18], [19] is modified and improved for seamless mode transfers. The contributions of this paper are as follows. The controller design processes of the PR-based triple loop are described in detail considering the system stability and transient dynamics. The proposed method is based on the stationary reference frame and is basically designed by combining an improved grid-synchronization technique [19] with the concept of a limiter [14], [17] to realize seamless mode transfers under all mode change events. The method includes both intentional islanding and the unintentional islanding caused by the sudden opening of a recloser switch during grid fault events. In [17], the load voltage magnitude in the islanded mode was regulated by the threshold value of a limiter due to saturation of the outer-grid current loop. Therefore, the voltage in the islanded mode was not satisfactory and additional control techniques were necessary to improve the load-voltage quality. A seamless mode-transfer technique can counter this problem by using a technique that properly changes the feedforward reference voltage according to specific operation modes. This method can improve voltage quality in the islanded mode to rated magnitude and frequency values. The proposed method is verified by PSiM simulations and laboratory-scale VDER-HILS experiments.

II. CONTROLLER DESIGN

Fig. 3 shows the configuration of the utility interactive inverter circuit and a control block diagram of the indirect current controller in the steady-state of the grid-connected mode. It includes 3-step control loops that consist of a grid-side current-control loop, a middle capacitor-voltage control loop, and an inner inverter-side inductor current loop [8]. To make seamless mode transitions possible, the output load voltage, which is the same as the capacitor voltage, should be controlled consistently in all of the operation modes. Therefore, the performance of the seamless mode transition mainly depends on how robustly the multi-loop output voltage controller is designed. Based on the previously designed robust multi-loop voltage controller, the outer-grid current control loop can be designed with a proper control bandwidth.

Fig. 4 shows a control block diagram and the root locus of the inner current-control loop. Fig. 4(a) presents a control block diagram of the inner current controller, where K_{P_Ii} and K_{pwm} are the proportional gain of the current controller and

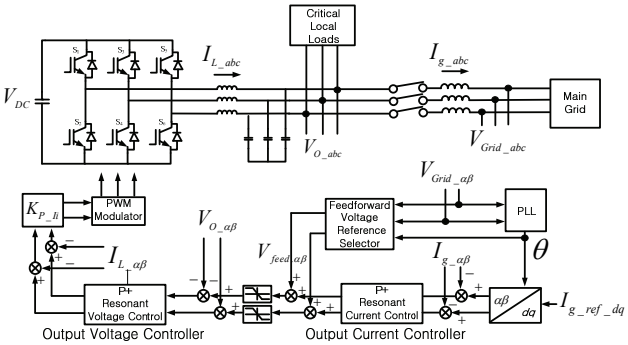

Fig. 3. Configuration of utility interactive inverter circuit and indirect current controller.

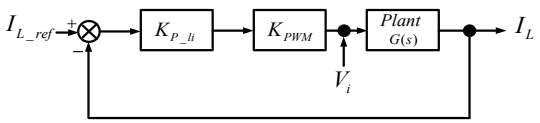

(a)

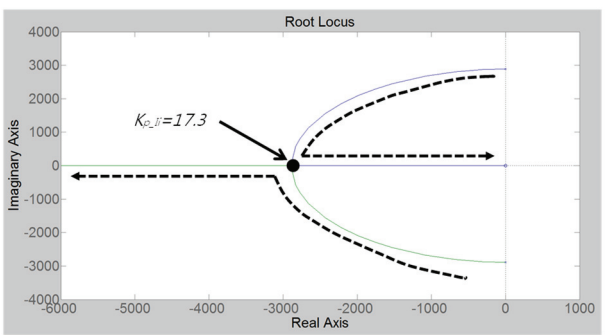

(b)

Fig. 4. Inner current-control loop: (a) Block diagram; (b) Root locus.

the pulse-width modulation (PWM) gain of the inverter, respectively. *G(s)* is the LC filter transfer function when the output current, I_o, is assumed to be the disturbance, which can be described by equation (1):

$$G(s)=\frac{I_L(s)}{V_i(s)}=\frac{sC}{s^2LC+1} \tag{1}$$

Considering the LC filter transfer function of equation (1), the closed transfer function of the current controller can be expressed as equation (2):

$$\frac{I_L(s)}{I_{L\_ref}(s)}=\frac{sK_{P\_Ii}K_{PWM}C_f}{s^2L_iC_f+sK_{P\_Ii}K_{PWM}C_f+1} \tag{2}$$

Fig. 4(b) shows the root locus of the closed-loop transfer function of the current controller in equation (2) according to different values of K_{P_Ii} when the PWM gain of the inverter, K_{pwm}, is assumed to be 1. As shown in this figure, all of the oscillation characteristics can be completely eliminated when K_{P_Ii} is bigger than 17.3 [22].

Fig. 5 shows a block diagram of the middle voltage loop, which includes an inner current loop. Based on this diagram, the characteristic equation of the voltage loop can be calculated

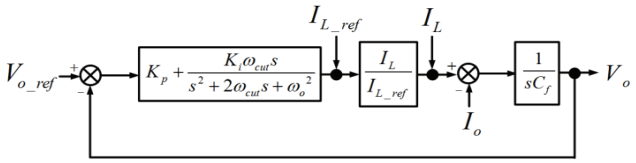

Fig. 5. Block diagram of middle voltage loop, which includes inner current loop.

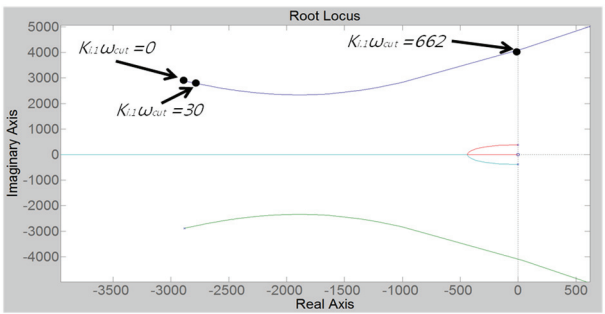

Fig. 6. Root locus for various values of fundamental resonant gain $K_{i.1}\cdot\omega_{1.cut}$ with $K_p = 0.0577$.

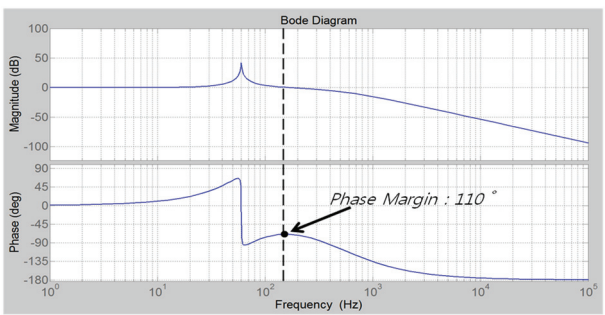

Fig. 7. Open-loop bode plot of PR-based voltage controller: K_p = 0.0577, $K_{i.1}\cdot\omega_{1.cut}$ = 30.

from the closed-loop transfer function as equation (3).

To select the gains of the PR voltage loop using the characteristic equation, the same method proposed in [9], where the other gain is assumed to be zero, is used. As a result, both of the gains are selected using the root locus analysis based on the gain selection criteria. The proportional gain is chosen to obtain a damping ratio, ξ, of 0.707, and the resonant gain is chosen to obtain a damping ratio, ξ, of 1 to avoid affecting the system transient dynamics (the proportional control gain mainly affects the system transient dynamics in the PR control [23]-[25]).

To analyze the characteristics of the full system, a root locus analysis is carried out, as shown in Fig. 6, for different resonant gains, $K_{i.1}\cdot\omega_{1.cut}$, with a fixed proportional gain, K_p, of 0.0577. As shown in this figure, the resonant gain varies from zero to several hundred. However, the slope remains at a similar value (the slope represents the damping ratio). Therefore, the dynamic transients of the PR voltage controller are mainly affected by the proportional gain [23]-[25].

Fig. 7 shows an open-loop bode plot of the PR-based middle voltage controller. The controller is designed to have a large gain at the center frequency of 60 Hz with a phase margin of 110°, which guarantees stable control operation. If 5th or 7th harmonic resonant controllers are added to the voltage loop, the phase margin can be reduced when the harmonic resonant gains increase. However, only the fundamental component based control loop is used in this paper since the focus of this study is seamless mode transfers.

Fig. 8 shows a control block diagram of the outer-grid current loop, which includes a middle capacitor voltage loop. Fig. 9 shows a Bode plot of the closed-loop transfer function of the outer-grid current loop. The bandwidth of the outer-grid current loop is designed as 367 Hz, which is within 1/20 of the switching frequency of 10 kHz. Therefore, a tradeoff is necessary between the control margin and the dynamic control performance.

III. Proposed Mode Transfer Method Based on Indirect Current Control

The mode transfer method using PR-based indirect current control is described for a line interactive inverter as shown in Fig. 10. The local load is connected to the capacitor port of the LCL filter, which is connected to the grid through two switches. The switch S_i is located between the local load and the grid-side inductor, L_g, and the switch S_g is located between the switch S_i and the main grid.

Fig. 11 presents an overall control block diagram of the proposed control method. The whole control structure

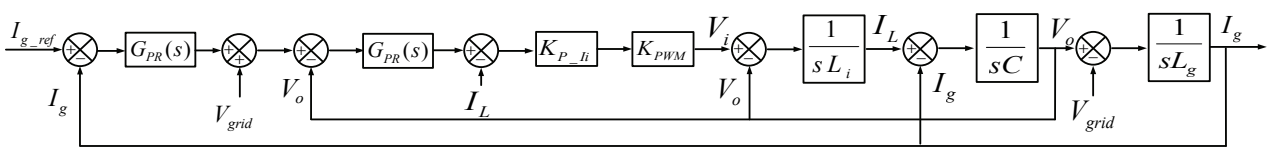

Fig. 8. Block diagram of whole indirect current loop.

$$\frac{V_o}{V_{o\_ref}} = \frac{s^2 K_p K_{P\_Ii} + s(2K_p K_{P\_Ii}\omega_{cut} + K_i K_{P\_Ii}) + K_p K_{P\_Ii}\omega_o^2}{s^4 LC + s^3(K_{P\_Ii}C + 2LC\omega_{cut}) + s^2(2\omega_{cut}K_{P\_Ii}C + K_p K_{P\_Ii} + LC\omega_o^2 + 1) + s(K_{P\_Ii}C\omega_o^2 + K_i K_{P\_Ii} + (K_p K_{P\_Ii} + 1)2\omega_{cut}) + (K_p K_{P\_Ii} + 1)\omega_o^2} \quad (3)$$

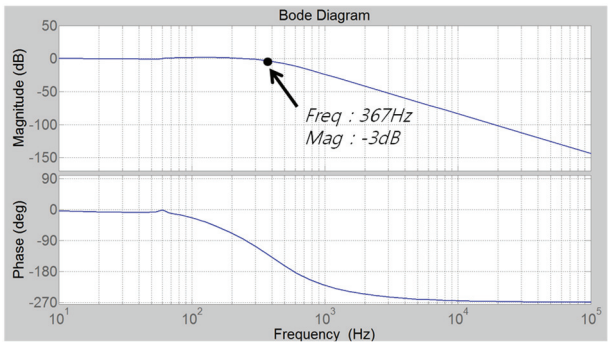

Fig. 9. Bode plot of closed-loop transfer function of outer-grid current loop.

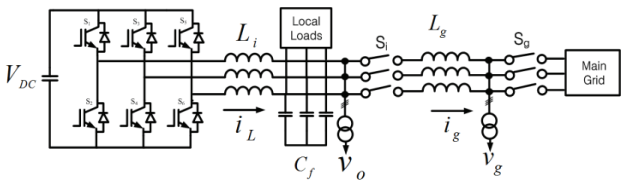

Fig. 10. Configuration of utility interactive inverter circuit with local loads.

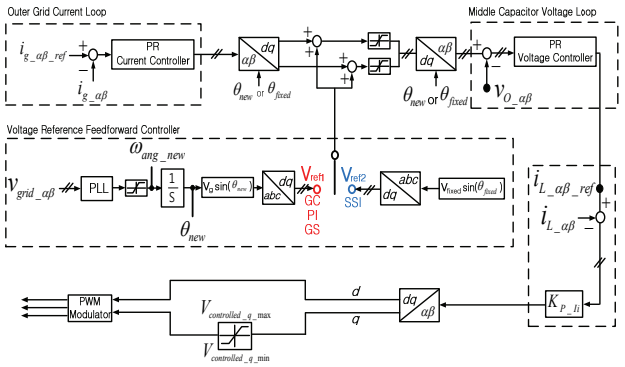

Fig. 11. Overall control block diagram of proposed control method.

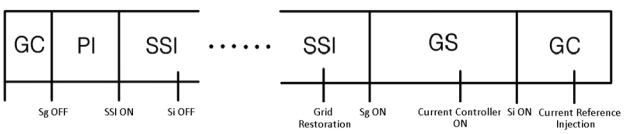

(a) (b)

Fig. 12. Mode-transfer sequences: (a) Mode transfer from grid-connected mode to islanded mode; (b) Mode transfer from islanded mode to grid-connected mode.

consists of a control loop based on 3 steps, which includes the outer- grid current loop, the middle capacitor (local load) voltage loop, and the inner inverter-side inductor current loop. Unlike the indirect current control method proposed in [17], a feedforward control is applied to generate the reference voltage. The feedforward voltage control term is added to the output of the outer-grid current loop to obtain the final reference voltage for the middle loop.

Two substantial advantages can be obtained from this feedforward technique. Firstly, it can enhance the robustness and stability of the control. The feedforward reference voltage value becomes more dominant than the output value of the outer-grid current loop among all of the final reference voltage components. This means that the final control output can be less sensitive to output control variations of the outer-grid current loop. In other words, the reference voltage feedforward technique can reduce the control action of the outer-grid current loop [29]-[31]. Secondly, an improved seamless mode transition can be realized with the proper selection of the feed forward value according to the operation modes. As shown in Fig. 11, two kinds of reference voltages are used. The first one is obtained from the grid voltage for grid-connected operation, unintentional islanding operation, and synchronization with the grid through a phase-locked loop (PLL), which has limiter threshold values. Note that the grid voltage is directly injected into the feedforward term in the steady-state utility interactive operation. The second reference voltage is obtained from the fixed voltage magnitude and frequency of the steady-state islanded mode operation. The phase of the load voltage must be saved and renewed by the present phase of the grid voltage. A smoother reference voltage change can be realized from these two advantages.

The proposed control structure considers both intentional and unintentional islanding operations due to sudden openings of the recloser switch. As shown in Fig. 11, the final reference voltage value is limited by a properly designed limiter in the d-q synchronous reference frame. The limiter threshold value for the final reference voltage $V_{ref\_d\_max}$ of the d-axis is 1.1 times the rated phase-to-neutral voltage. The limiter threshold value $V_{ref\_q\_max}$ or min for the final reference voltage of the q-axis is set to ±10% of the rated grid voltage based on the study in [17].

The synchronous phase θ_{sync} also needs to be applied selectively according to the operation modes between θ_{new} and θ_{fixed}. After unintentional islanding occurs due to an opening of the recloser switch, the output of the outer-grid current loop is saturated due to an extreme increase in the grid current error. Therefore, the limiter can block this control failure and limit the final reference voltage to the threshold value based on the waveform.

Fig. 12 shows the whole mode transfer sequence with the proposed indirect current control. Fig. 12(a) shows a mode transition from the grid-connected mode to the islanded mode. The whole mode transfer sequence is same as the following: GC (grid connected mode) ⟶ PI (pre-islanded mode) ⟶ SSI (steady-state islanded mode). Fig. 12(b) shows the mode transition from the islanded mode to the grid-connected mode, which has the following mode transfer sequence: SSI ⟶ GS (grid synchronization mode) ⟶ GC again. The whole mode transfer sequence of the system can be established based on Figs. 10, 11 and 12. The proposed mode transfer sequence is described in detail as follows.

A. Mode Transfer from Grid-Connected Mode to Islanded Mode

Initially, the utility interactive inverter operates in the grid connected mode by supplying the local load and simultaneously delivering power to the main grid. If a grid fault occurs while the inverter operates in the grid-connected mode, the recloser switch, S_g, is opened to disconnect the DG-based inverter from the main grid as an anti-islanding scheme. The operation mode is automatically changed to the PI mode before receiving the islanding detection signals to prepare for the mode change to the islanded mode.

In the PI mode, the final reference voltage of the middle voltage loop is regulated by the limiter, which is located after the feedforward terms of the d-q reference voltages in Fig. 11. Even though the magnitude of the reference voltage is consistently maintained at the limiter threshold, the output voltage is beyond the rated voltage [17]. Therefore, after the arrival of the anti-islanding detection signal, the inverter mode is changed to the SSI mode by toggling the mode selection switch in Fig. 11 to simultaneously apply the internal reference voltage and open the inverter switch, S_i. At the start of the SSI mode, the outer grid loop must also be disabled to avoid being useless for the control action. The integrated output variable of the resonant controller is a sequence of output values (n), (n-1) and (n-2), which must be reset to zero to counter the saturation of the resonant controller due to the increasing error of the outer-grid current loop when unintentional islanding occurs.

In the SSI mode, a fixed voltage magnitude and frequency are adopted by toggling the mode selection switch to improve the load voltage quality. The phase information is saved and renewed as the present sensed voltage phase. As a result, the constant-voltage and constant-frequency operations can start from this saved initial phase value when the mode changes to the SSI mode.

B. Mode Transfer from Islanded Mode to Grid-Connected Mode

When the grid is restored from a fault condition, the inverter mode needs to change from the SSI mode to the GC mode. For the mode transfer, the inverter output voltage must be synchronized to the grid voltage through the GS mode. After detecting the grid restoration signal, the recloser, S_g, is closed. Then the grid voltage can be sensed. A previous method for modification of the GS mode reference can be used for seamless grid synchronization in the stationary reference frame [19]. The limiter design of a PLL is proposed in consideration of the compatibility between the limiter threshold value and the allowable frequency range of the fundamental resonant control. Therefore, both the resonant frequency, ω_{cut}, of the fundamental resonant controller and the angular frequency variation range of the PLL are chosen to be 6 rad/s.

After the grid synchronization is complete, the inverter mode needs to be changed to the GC mode. However, before connecting to the main grid, the outer-grid current loop has to be enabled. No transition occurs because of the zero grid current $I_{g\_\alpha\beta}$, and the initial value of zero assigned as the reference grid current, $I^*_{g\_\alpha\beta\_ref}$. In other words, the output of the outer current loop can be zero due to the zero value of the outer grid-current error. For the change to the GC mode, the switch S_i is closed. Then operation in the GC mode finally starts. The steady-state operation in the grid-connected mode can be achieved by smoothly changing the magnitude of the reference grid current to its rated value with a ramp function.

TABLE I
SIMULATION PARAMETERS

Symbols	Meanings	Values
I_{Peak}	Peak grid current	9.5 A
V_{dc}	DC link voltage	400 V
f_{sw}	Switching frequency	10 kHz
V_{rated}	Rated output voltage	105 V
L_i, L_g	Filter inductance	3, 1 mH
C_f	Filter capacitor	40 (Y)
K_{p_Ii}	Proportional gain of *IL* Loop	17.3
K_p	Proportional gain of *Vo* Loop	0.0577
K_{p_Io}	Proportional gain of *Ig* Loop	2
$K_i \cdot \omega_{cut}$	Resonant gain of *Vo* Loop	30
$K_{ii.1} \cdot \omega_{1.cut}$	Resonant gain of *Ig* Loop	100

IV. SIMULATION RESULTS

Table I shows the simulation parameters for the utility interactive inverter. The system configuration and control scheme are based on Figs. 10 and 11. The Δ-Y transformer is located at a point between the local load and the grid to synchronize the inverter output voltage to the grid voltage. The sampling frequency is 20 kHz, and the switching frequency is 10 kHz which is half the sampling frequency.

The steady-states of the SSI and GC modes as well as the transient state of the mode changes from GC to SSI and from SSI to GC are shown from Fig. 13 to Fig. 17. Figs. 13 and 14 show the steady-state simulation results of the SSI and GC modes. The output load voltage is well regulated with a 1.7% total harmonic distortion (THD) in the SSI mode, as shown in Fig. 13. The output load voltage and the grid current are also well regulated with 1.8% and 1.6% THDs in the GC mode as shown in Fig. 14. These results verify the performance of the gain selection criteria. Fig. 15 shows simulation results for all of the operation modes during mode changes from GC to SSI and from SSI to GC. The output load voltage can be regulated in all of the changes of operation mode with the proposed control technique. The detailed performance of each mode transition event is shown in the following figures.

Fig. 16 shows the simulation results when the mode changes from GC to SSI due to the sudden opening of S_g. The inverter

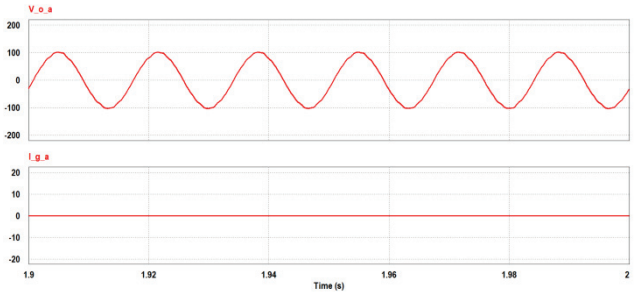

Fig. 13. Simulation results in SSI mode: (top) Measured load voltage; (bottom) measured grid current (THD: V_o (1.7%)).

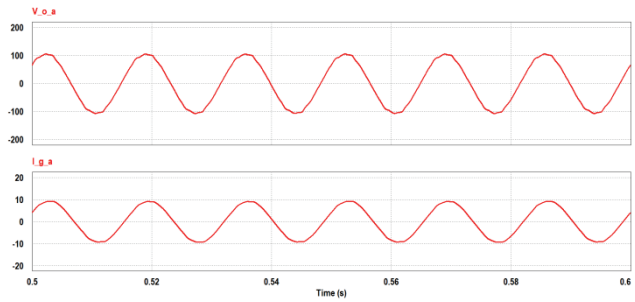

Fig. 14. Simulation results in GC mode: (top) Measured load voltage; (bottom) measured grid current (THD: V_o (1.8%), I_g (1.6%)).

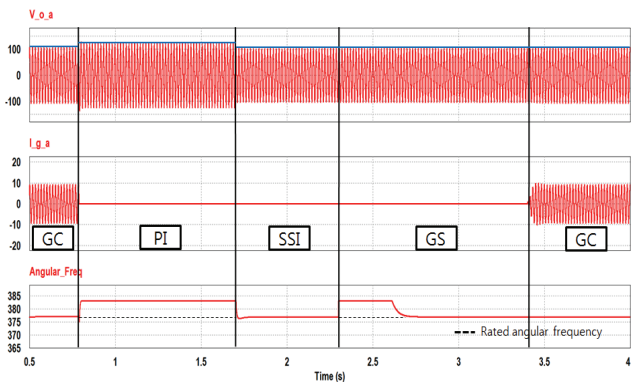

Fig. 15. Simulation results for all of operation modes during mode changes: (top) Measured load voltage; (middle) measured grid current; (bottom) angular frequency of the load voltage.

is initially operated in the GC mode. Then the inverter operation mode changes from GC to PI when the recloser switch S_g opens due to the occurrence of a grid fault. In this mode, the load voltage is maintained with the threshold value of the limiter, which is located at the final summing point of the reference voltage. However, the output voltage is beyond the rated voltage range. Therefore, after the arrival of the anti-islanding detection signal, the inverter mode is changed to the SSI mode by toggling the mode selection switch to simultaneously apply the internal reference voltage and open the inverter switch S_i. When the SSI mode starts, the outer grid loop must also be disabled to avoid useless control actions. Therefore, the PI mode is only used for the transient state during the mode change from GC to SSI.

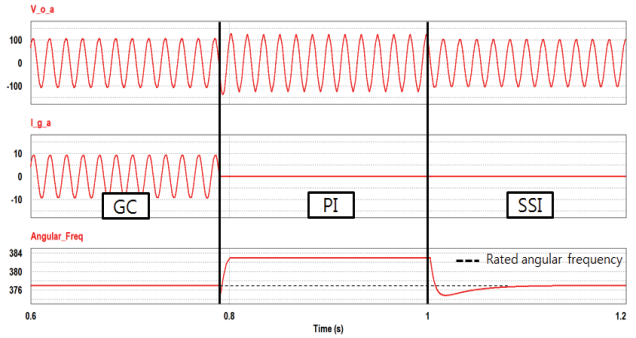

Fig. 16. Simulation results of mode changes from GC to SSI: (top) Measured load voltage; (middle) measured grid current; (bottom) angular frequency of the load voltage.

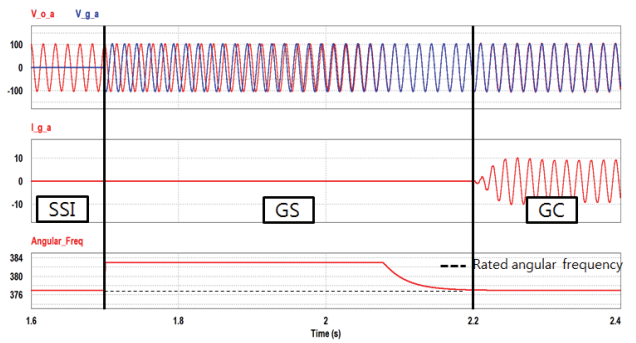

Fig. 17. Simulation results of mode changes from SSI to GC: (top) Measured load voltage and measured grid voltage; (middle) measured grid current; (bottom) angular frequency of the load voltage.

Fig. 17 shows simulation results of the mode changes from SSI to GC when the grid is restored from a grid fault. If the recloser switch, S_g, is closed at 1.7 s, the mode changes to the GS mode to track the phase of the restored grid voltage. The grid synchronization starts at 1.7 s, and the load voltage smoothly tracks the phase of the grid voltage within the limited threshold value of the PLL's angular frequency. After the grid synchronization is complete, the outer-grid current loop is enabled at 2.18 s to stand by the GC mode. Note that there is no control action for the outer-grid current loop since the reference grid current and measured value are all zero, which results in a control output of zero. When the inverter switch, S_i, is on, the inverter is changed to the GC mode by assigning the rated grid current reference at 2.2 s.

V. Experimental Results

Table II shows the experimental parameters. Most of the parameter values are the same as the simulation parameters except for the peak grid current and DC link voltage due to the limited power capacity of the system in the laboratory experimental setup.

Fig. 18 shows the laboratory-scale experimental setup based on VDER-HILS. In this experiment, the proposed methods are verified using only AC-based systems, such as a static

TABLE II
EXPERIMENTAL PARAMETERS

Symbols	Meanings	Values
I_{Peak}	Peak grid current	5 A
V_{dc}	DC link voltage	360 V
F_{sw}	Switching frequency	10 kHz
V_{rated}	Rated output voltage	105V
L_i, L_g	Filter inductance	3, 1 mH
C_f	Filter capacitor	40(Y)
K_{p_Ii}	Proportional gain of I_L Loop	17.3
K_p	Proportional gain of V_o Loop	0.0577
K_{p_Io}	Proportional gain of I_g Loop	2
$K_r \cdot \omega_{cut}$	Resonant gain of V_o Loop	30
$K_{ii.r} \cdot \omega_{I.cut}$	Resonant gain of I_g Loop	100

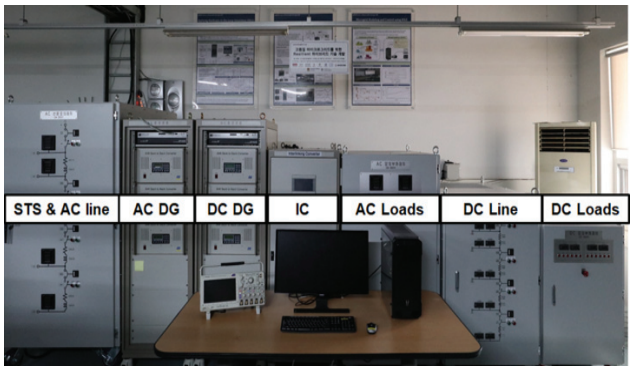

Fig. 18. Experimental setup based on VDER-HILS.

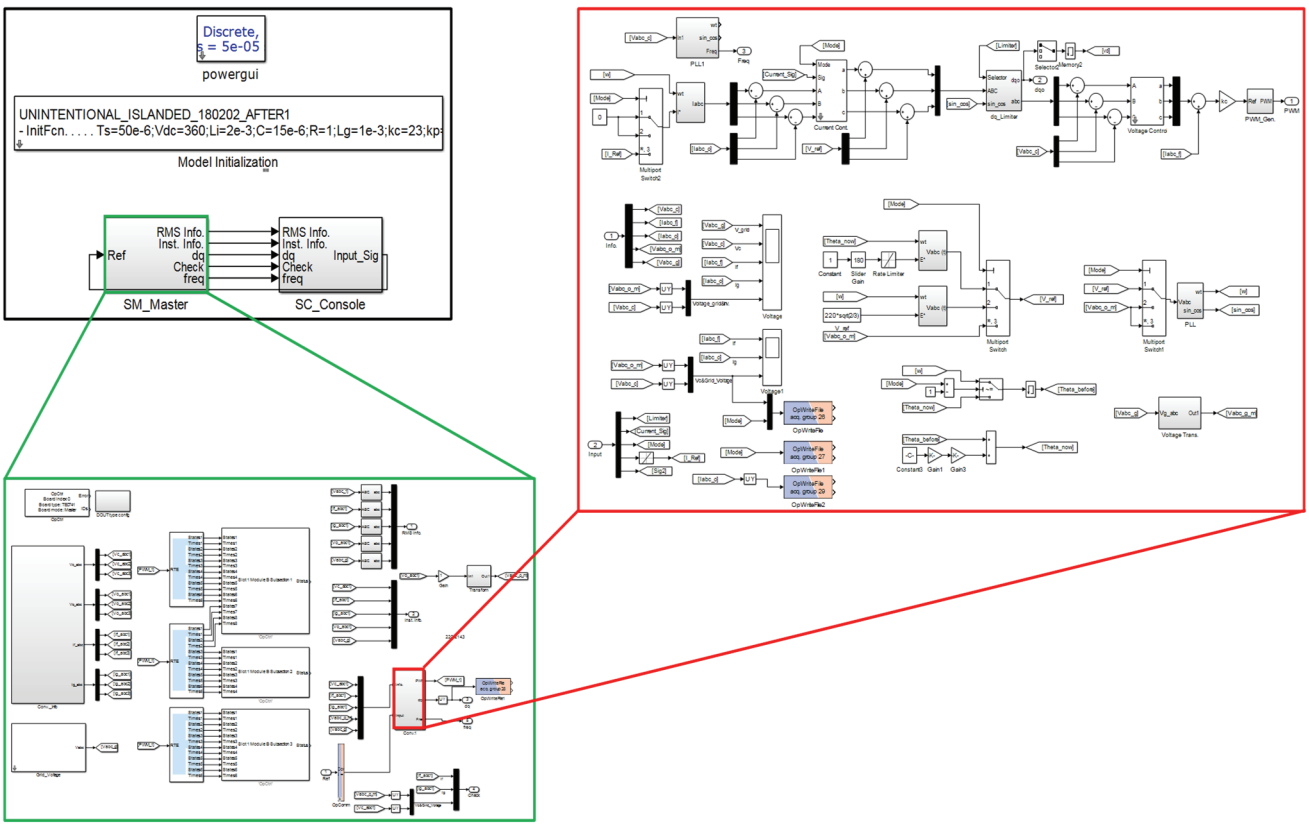

Fig. 19. Controller design to operate VDER-HILS based on MATLAB Simulink.

transfer switch (STS), AC line, distributed generator (AC DG) and AC loads. Fig. 19 shows the controller design based on MATLAB Simulink which is combined with the HILS system. MATLAB Simulink can interface with the HILS as a main controller to operate the system.

Fig. 20 shows experimental results of a mode change from GC to SSI through the PI mode in consideration of unintentional islanding resulting from an opening of the recloser switch, S_g, due to a grid fault. Initially, the inverter is operated in the steady-state of the GC mode to supply current to the grid. After S_g is opened, the operation mode changes from GC to PI. In the PI mode, the output voltage is regulated by the threshold value of the reference-voltage limiter in spite of the grid current error. After the anti-islanding detection signal arrives, the inverter operation mode is changed to SSI by toggling the mode-selection switch. Then the output load voltage is controlled to follow the internal reference-voltage mode to obtain a better load voltage magnitude and frequency regulation performance in the islanded mode. When SSI starts, the outer grid loop is disabled to avoid useless control actions in the SSI mode. The proposed reference feedforward controller eventually changes the mode smoothly by reducing the influence of the outer grid current controller.

Fig. 21 shows the grid synchronization performance in the

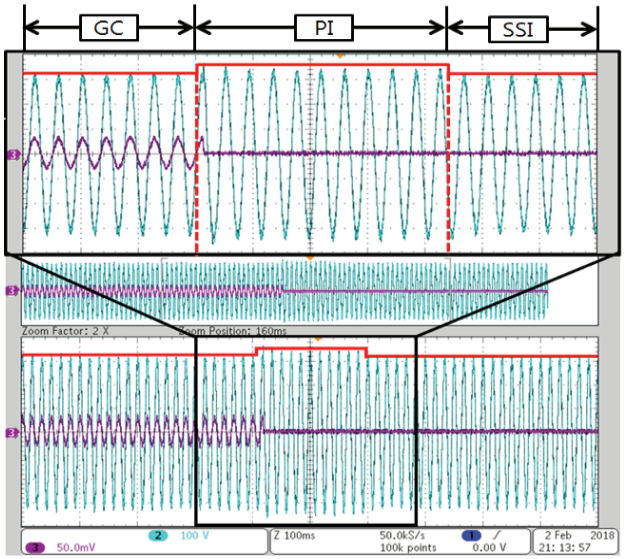

Fig. 20. Mode transfer performance with unintentional islanding: (purple) Measured grid current (5A/div); (light blue) measured load voltage (100 V/div).

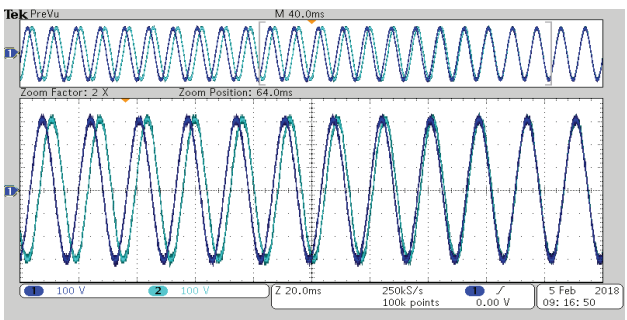

Fig. 21. Grid synchronization performance in GS mode: (dark blue) Measured load voltage (100 V/div); (light blue) measured grid voltage (100 V/div).

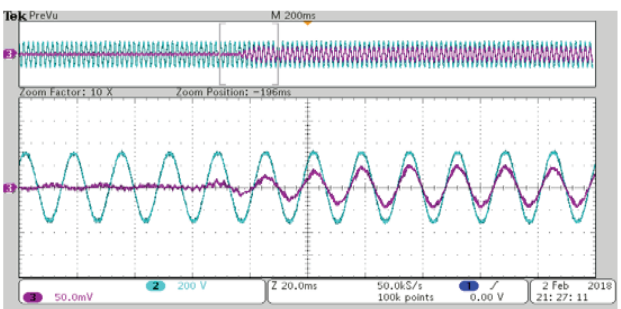

Fig. 22. Experimental results when reference grid current changes with ramp function: (purple) Measured grid current (5 A/div); (light blue) measured load voltage (100 V/div).

GS mode to track the load voltage with the phase of the grid synchronization method that considers the mutual compatibility between the frequency change and the allowable control range of the PR controller [19]. However, fast synchronization is not preferable because it may exceed the allowable limit of voltage. The proposed mode-transfer technique includes a grid the load frequency due to instantaneous frequency changes. Therefore, the frequency limit and cut-off frequency ω_{cut} are selected as 6 rad/s to realize seamless grid synchronization. After the grid synchronization is complete, the blocked outer-grid current loop output is re-enabled to enter the GC mode. No transient effect occurs because both the reference and measured values of the grid current loop are zero so that the grid current error is zero, which causes the zero control output of the outer-grid current loop.

Finally, the inverter enters the GC mode by closing the inverter switch S_i, and the grid current can be controlled to follow the rated reference value. Fig. 22 shows experimental waveforms of the grid voltage and the grid current. However, as shown in this figure, it takes time for the grid current to reach the rated value since the reference is assigned to increase smoothly to realize a smooth dynamic response.

VI. Conclusions

In this study, a seamless mode transfer method that uses the PR-based indirect current control is investigated for the operation of utility interactive inverters. The proposed method can realize seamless mode transitions in all of the inverter operation modes including the unintentional islanding mode. Additionally, the quality of the load voltage in the steady-state islanded mode can be improved to the rated value in contrast to the unrated value in previous works. This is achieved by adding a feedforward voltage-selection technique to the output of the grid current loop. The proposed method is validated through results obtained with PSiM simulations and an experimental setup based on VDER-HILS.

Acknowledgment

This work was supported by the Korea Institute of Energy Technology Evaluation and Planning (KETEP) and the Ministry of Trade, Industry & Energy (MOTIE) of the Republic of Korea (No. 20168530050030).

References

[1] *Distributed Generation with High Penetration of Renewable Energy Sources* (DISPOWER), http://www.dispower.org.

[2] *Distributed Intelligence in Critical Infrastructures for Sustainable Power* (CRISP), http:// www. crisp. ecn. nl.

[3] *Distributed generation at Lawrence Berkeley National Laboratory* (LBNL), http://der.lbl.gov.

[4] *The Consortium for Electric Reliability Technology Solutions* (CERTS), http://certs.lbl.gov.

[5] *The Grid Wise alliance*, http://www.gridwise.org/.

[6] *Large Scale Integration of Micro-generation to Low Voltage Grids* (MICROGRIDS), http://microgrids.power.ece.ntua.gr.

[7] *IEEE Standard for Interconnecting Distributed Resources*

with Electric Power Systems, IEEE Standard 1547, 2003.
[8] K. Lim, J. Jang, J. Lee, J. Kim, and J. Choi, "P+ multiple resonant control for output voltage regulation of microgrid with unbalanced and nonlinear loads," in *Proc. of IPEC'2014 -ECCE Asia*, 21G2-2, 2014.
[9] K. Lim, J. Jang, S. Moon, J. Kim, and J. Choi, "Output voltage regulation based on P plus resonant control in islanded mode of microgrids," in *Proc. of PEMC'2014*., pp. 452-457, 2014.
[10] F. S. Pai, "An improved utility interface for micro turbine generation system with stand-alone operation capabilities," *IEEE Trans. Ind. Electron*., Vol. 53, No. 5. pp. 1529-1537, Oct. 2006.
[11] R. Teodorescu and F. Blaabjerg, "Flexible control of small wind turbines with grid failure detection operating in stand-alone and grid-connected mode," *IEEE Trans. Power Electron.*, Vol. 19, No. 5. pp. 1323-1332, Sep. 2004.
[12] I. J. Balaguer, Q. Lei, S. Yang, U. Suppati, and F. Z. Peng, "Control for grid-connected and intentional islanding operations of distributed power generation," *IEEE Trans. Ind. Electron*., Vol. 58, No. 1, pp. 147-157, Jan. 2011.
[13] Y. Li, D. M. Vilathgamuwa, and P. C. Loh, "Design, analysis, and realtime testing of a controller for multibus microgrid system," *IEEE Trans. Power Electron.*, Vol.19, No.5. pp. 1195-1204, Sep. 2004.
[14] J. Kwon, S. Yoon, and S. Choi, "Indirect current control for seamless transfer of three-phase utility interactive inverters," *IEEE Trans. Power Electron*., Vol. 27, No. 2, pp. 773-781, Feb. 2012.
[15] S. Yoon, H. Oh, and S. Choi, "Controller design and implementation of indirect current control based utility-interactive inverter system," *IEEE Trans. Power Electron*., Vol. 28, No. 1, pp. 26-30, Jan. 2013.
[16] Z. Liu, J. Liu, and Y. Zhao, "A Unified control strategy for three-phase inverter in distributed federation," *IEEE Trans. Power Electron*., Vol. 29, No. 3, pp. 1176-1191, Mar. 2014.
[17] Z. Liu and J. Liu, "Indirect current control based seamless transfer of three-phase inverter in distributed generation," *IEEE Trans. Power Electron*., Vol. 29, No. 7, pp. 3368-3383, Jul. 2014.
[18] K. Lim and J. Choi, "PR based indirect current control for seamless transfer," in *Conf. Rec. of IPEMC'2016-ECCE Asia*, 2016.
[19] K. Lim and J. Choi, "Seamless grid synchronization of a proportional + resonant control-based voltage controller considering non-linear loads under islanded mode," *Energies*, Vol. 10, No. 10, 2017.
[20] D. De and V. Ramanarayanan, "A proportional + multi resonant controller for three-phase four-wire high-frequency link inverter," *IEEE Trans. Power Electron*., Vol. 25, No. 4. pp. 899-906, Apr. 2010.
[21] D. De and V. Ramanarayanan, "Decentralized parallel operation of inverters sharing unbalanced and nonlinear loads," *IEEE Trans. Power Electron.*, Vol. 25, No. 12. pp. 3015-3025, Dec. 2010.
[22] K. Lim and J. Choi, "Output voltage regulation for harmonic compensation under islanded mode of microgrid," *Journal of Power Electron.*, Vol. 17, No. 2, pp. 464-475, Mar. 2017.
[23] F. Blaabjerg, R. Teodorescu, M. Liserre, and A. Timbus, "Overview of control and grid synchronization for distributed power generation system," *IEEE Trans. Ind. Electron*., Vol. 53, No. 5, pp. 1398-1409, Oct. 2006.
[24] D. N. Zmood, D. G. Holmes, and G. H. Bode, "Stationary frame current regulation of PWM inverters with zero steady-state error," *IEEE Trans. Power Electron*., Vol. 18, No. 3, pp. 814-822, May 2003.
[25] D. N. Zmood, D. G. Holmes, and G. H. Bode, "Frequency domain analysis of three-phase linear current regulators," *IEEE Trans. Ind. Appl*., Vol. 37, No. 2, pp. 601-610, Mar./ Apr. 2001.
[26] W. Feng, K. Sun, Y. Guan, J. M. Guerrero, and X. Xiao, "The frequency fluctuation impact analysis for droop controlled grid-connecting inverter in microgrid," in *Proc. of IPEMC'2016- ECCE Asia*, 2016.
[27] Y. Guan, J. C. Vasquez, and J. M. Guerrero, "Hierarchical controlled grid-connected microgrid based on a novel autonomous current sharing controller," in *Proc. of ECCE' 2015- ECCE Asia*, pp. 2333-2340, 2015.
[28] T. Ye, N. Y. Dai, and C. S. Lam, "Analysis, design, and implementation of a quasi-proportional-resonant controller for a multiplication capacitive-coupling grid-connected inverter," *IEEE Trans. Ind. Appl*., Vol. 52, No. 5, pp. 4269-4279, Sep./Oct. 2016.
[29] M. J. Ryan, R. W. D. Doncker, and R. D. Lorenz, "Decoupled control of a four-leg inverter via a new 4X4 transformation matrix," *IEEE Trans. Power Electron*., Vol. 16, No. 5, pp. 694-701, Sep. 2001.
[30] M. J. Ryan, W. E. Brumsickle, and R. D. Lorenz, "Control topology options for single-phase UPS inverters," *IEEE Trans. Ind. Appl*., Vol. 33, No. 2, pp. 493-501, Mar./Apr. 1997.
[31] P. C. Loh, M. J. Newman, D. N. Zmood, and D. G. Holmes, "A comparative analysis of multi-loop voltage regulation strategies for single and three-phase UPS systems," *IEEE Trans. Power Electron*., Vol. 18, No. 5, pp. 1176-1185, Sep. 2003.

Kyungbae Lim was born in Korea, in 1985. He received his B.S., M.S. and Ph.D. degrees in Electrical Engineering from Chungbuk National University, Cheongju, Korea, in 2011, 2013 and 2017, respectively. From 2017 to 2018, he worked as a Postdoctoral Researcher at the BK21 Chungbuk Information Technology Center, Chungbuk National University. His current research interests include the seamless mode transfer of utility interactive inverters.

Injong Song was born in Korea, in 1992. He received his B.S. degree from the School of Electrical Engineering, Chungbuk National University, Cheongju, Korea, in 2013, where he is presently working towards his M.S. degree in the School of Electrical Engineering. His current research interests include power quality improvements for parallel inverter operation.

Jaeho Choi received his B.S., M.S. and Ph.D. degrees from the Department of Electrical Engineering, Seoul National University, Seoul, Korea, in 1979, 1981 and 1989, respectively. From 1981 to 1983, he was a full time Lecturer at the Jungkyoung Technical College, Daejeon, Korea. Since 1983, he has been with the School of Electrical Engineering, Chungbuk National University, Cheongju, Korea, where he is presently working as a Professor. In 1993, 1998, 2003 and 2009 he was a Visiting Professor at the University of Toronto, Toronto, Canada. He was a Danfoss Visiting Professor at the Aalborg University, Aalborg, Denmark, in 2000 and he was also a Visiting Professor at the Bandung Institute of Technology, Bandung, Indonesia, in 2017. His current research interests include power electronics, power quality problems and solutions, energy storage systems, and renewable energy and microgrid systems. He is an active Member of KIEE, KIPE and IEEE. He was the Editor-in-Chief of the JPE and the President of KIPE.

Hyeong-Jun Yoo received his Ph.D. degree in Electrical Engineering from Incheon National University, Incheon, Korea, where he is presently working as a Postdoctoral Researcher. His current research interests include the control of power conversion systems, microgrids and dc distribution systems.

Hak-Man Kim received his first Ph.D. degree in Electrical Engineering from Sungkyunkwan University, Suwon, Korea, in 1998; and his second Ph.D. degree in Information Sciences from Tohoku University, Sendai, Japan, in 2011. From October 1996 to February 2008, he worked for the Korea Electrotechnology Research Institute (KERI), Ansan, Korea. He is presently working as a Professor in the Department of Electrical Engineering, Incheon National University, Incheon, Korea. His current research interests include microgrid operation and control, and DC power systems.